

HO_x measurements in the summertime upper troposphere over Europe: A comparison of observations to a box model and a 3D model.

E. Regelin¹, H. Harder¹, M. Martinez¹, D. Kubistin^{1*}, C. Tatum Ernest¹, H. Bozem^{1**}, T. Klippel¹, Z. Hosaynali-Beygi¹, H. Fischer¹, R. Sander¹, P. Jöckel^{1***}, R. Königstedt¹, J. Lelieveld¹

¹ Department of Atmospheric Chemistry, Max Planck Institute for Chemistry, Mainz, Germany

* now at: University of Wollongong, School of Chemistry, Wollongong, NSW, Australia

**now at: Institute for Atmospheric Physics, University Mainz, Germany

*** now at: Deutsches Zentrum für Luft und Raumfahrt (DLR), Institut für Physik der Atmosphäre, Oberpfaffenhofen, Germany

In-situ airborne measurements of OH and HO₂ with the HORUS (HydrOxyl Radical measurement Unit based on fluorescence Spectroscopy) instrument were performed in the summertime upper troposphere across Europe during the HOOVER 2 (HO_x OVer EuROpe) campaign in July 2007. Complementary measurements of trace gas species and photolysis frequencies were conducted to obtain a broad data set, which has been used to quantify the significant HO_x sources and sinks. In this study we compare the in-situ measurement of OH and HO₂ with simulated mixing ratios from the constrained box model CAABA/MECCA (Chemistry As A Box Model Application/Module Efficiently Calculating the Chemistry of the Atmosphere), and the global circulation model EMAC (ECHAM5/MESSy Atmospheric Chemistry Model). The constrained box model reproduces the observed OH and HO₂ mixing ratios with better agreement (obs/mod median 98 % OH, 96 % HO₂) than the global model (median 76 % OH, 59 % HO₂). The observations and the computed HO_x sources and sinks are used to identify deviations between the models and their impacts on the calculated HO_x budget.

1. Introduction

A wide range of chemical compounds emitted by human activities such as industrial processes and traffic, and by vegetation and animals, are oxidised by reactions with the OH radical. Short lived species are readily oxidised within the planetary boundary layer. Species with a longer lifetime can be mixed and diluted into the free and upper troposphere. There, some gases like HCHO and H₂O₂ form OH and HO₂ (together called HO_x) through photolysis; other species are depleted by reactions with OH.

The oxidation capacity of the atmosphere is formed by highly reactive species, which together act as the cleansing agents of the troposphere. The OH radical is the most important oxidising component of the troposphere and has been recognized as the most important cleansing oxidant (Levy,

1971). In the presence of NO_x or ozone, the OH reaches equilibrium with HO₂ and particularly NO shifts the HO_x equilibrium towards the OH.

The basic HO_x chemistry in the (upper) troposphere has previously been summarized in a number of articles (amongst others: Jaegle et al., 2000; Prather and Jacob, 1997; Ren et al., 2008). For the scope of this paper a limited number of HO_x production and loss channels are relevant. The most important tropospheric primary HO_x source is the photolysis of ozone and the subsequent reaction of O(¹D) with gas phase water (R 1 & 2, see Table 1). In the dry air masses of the upper troposphere, where the O(¹D)-water-reaction is relatively ineffective, photolysis of peroxides (R 3 & 4) and aldehydes (R 5 - 7) in particular HCHO, lead to substantial OH formation.

This can be important in addition to the $O(^1D)/H_2O-OH$ source and under some conditions becomes the dominant primary source (Jaegle et al., 2000; Ren et al., 2008; Tan et al., 2001).

HO_x radicals react with a large range of trace gases. Under low NO_x conditions in upper tropospheric background air the most important HO_x sink is the radical-radical-reaction of HO_2 either with a second HO_2 radical (R 9) or an organic RO_2 radical (R 10). The resulting peroxides are in turn precursor species of OH (Klippel et al., 2011), though in the presence of clouds, they are efficiently scavenged (Lelieveld and Crutzen, 1990; Snow et al., 2007). It was reported that, subsequent to the uptake and aqueous phase chemistry, soluble species such as peroxides and HCHO can be released again from cloud droplets through evaporation, as most clouds evaporate rather than precipitate. The micro-physical processes under freezing conditions are poorly understood and need further investigation. For example, there is ongoing discussion about H_2O_2 release from cloud droplets during freezing (Barth et al., 2001; Mari et al., 2000; Mari et al., 2002), which would increase H_2O_2 concentrations in the upper troposphere. Since the respective H_2O_2 was released from clouds it was not formed in-situ from HO_2 and therefore introduces a potential primary OH source.

A recent study (Klippel et al., 2011) reports that in comparison to field observations the global circulation model EMAC underestimates the H_2O_2 concentration in the upper troposphere over Europe. Here we investigate the implications of this underestimated H_2O_2

concentration in the global model on the HO_x -budget.

As shown by Tan et al. (2001) for the tropical Pacific, under upper tropospheric conditions a substantial fraction of the observed OH and HO_2 radicals is directly formed through primary production, whereas the dominant fraction is produced by cycling reactions. In general, the HO_x -equilibrium is determined by R 12 - 15. The variability of the HO_x -equilibrium is mainly influenced by the variability of the NO concentrations (R 12). Thus, increased or decreased OH mixing ratios can also be due to enhanced or reduced HO_2 cycling to OH. In the following sections, we will analyse the HO_x source and sink strengths with regard to primary and cycling HO_x sources in the upper troposphere under conditions observed during the HOOVER summer campaign. A comparison of a simple HO_x reaction scheme applied as part of a constrained box model and a global 3D model are used to identify differences, strengths, and weaknesses of the models.

The HOOVER 2 campaign is described in section 2. Technical details of the HO_x measurement instrument HORUS are given in section 3. Sections 4 and 5 present the box model and the global model, respectively. Results and discussion of the simulations are presented in the respective model section. The summary and conclusions are part of section 6.

2. The HOOVER 2 Campaign

The HOOVER 2 campaign was conceived to study the spatial variability of the oxidation capacity in the summertime troposphere over Europe (see also Klippel et al. 2011).

The most important oxidising species is the OH radical, which has been measured in-situ along with its precursors, the hydrogen peroxy radical, ozone, nitrogen monoxide, hydrogen peroxide and total organic peroxides (mean values are summarized in Table 2). To investigate the dominant species believed to impact the OH reactivity, methane, carbon monoxide, and formaldehyde were also measured.

An aircraft (Learjet 35 A) was used to conduct the measurements. A suite of measurement equipment was placed within the cabin and in wing pods which were mounted below the wings. Figure 1 shows a schematic overview of the payload. The wing pod which contained most of the HORUS instrument and infrastructure is shown in Figure 2.

Since all other instruments used in the study are described elsewhere, only a brief description is given here. Table 3 summarizes technical details of the measurement techniques used.

O₃ and NO were measured with a chemiluminescence (CL) detection system. This instrumental setup was already used in a similar configuration during the OOMPH campaign and is described in detail by Beygi et al. (2011).

H₂O₂ and organic peroxides were observed with a wet chemical system based on derivatisation and fluorescence enzyme (DEF) described in Klippel et al. (2011).

CO, CH₄ and HCHO measurements were performed with a multi-channel infrared quantum cascade laser (QCL) absorption spectrometer (Schiller et al., 2008).

J(NO₂) data was measured with a set of two filter radiometers (FR) for the down-welling and up-welling fraction.

H₂O was recorded with a Helten Sensor.

Here we report observations obtained during four flights between the Mediterranean (~ 41° N) and sub-polar Northern Scandinavia (~ 68° N), performed in the upper troposphere at altitudes higher than 7 km. Flight tracks are depicted in Figure 3. A typical profile of a HOOVER 2 flight is shown in Figure 4. During the campaign, the favoured flight level was above 7 km altitude in the upper troposphere and vertical profiles were sampled during takeoff and landing as well as during a midway descent during each flight.

3. HORUS instrument

a. Description

The OH and HO₂ radical concentrations were measured by using laser induced fluorescence, using the HORUS instrument, built at the Max-Planck-Institute for Chemistry in Mainz and redesigned for aircraft campaigns.

The laser system was located within the cabin of the Learjet, while the detection system and most of the infrastructure was mounted in a wing pod below one of the wings. The laser beam was transported into the detection system through 10 m long optical fibres.

UV light at about 308 nm was used to selectively excite OH radicals ($A^2\Sigma - X^2\Pi$, $v'=0 \leftarrow v''=0$) through the Q₁(2) transition in a low pressure detection cell (2 – 8 mbar). The laser pulse repetition frequency was set to 3 kHz during the HOOVER campaigns.

To increase the sensitivity of the instrument, the laser light was reflected 32 times using a White cell (White, 1942). Excitation and fluorescence occur at the same wavelength. The fluorescence was measured with a multi-channel photomultiplier perpendicular to the laser

beam. The background signal was determined by tuning the laser wavelength off-resonance of the excitation wavelength. The laser was tuned on- and off-resonance with the OH transition every 5 seconds to determine the fluorescence plus background signals and the background signals, respectively. The off-resonance background fluorescence was then subtracted from the on-resonance OH fluorescence signal. The achieved time resolution was 10 seconds.

OH was detected in a first axis. HO₂ was detected in a second axis 16 cm downstream of the first one after addition of NO titration gas to the air stream in order to convert HO₂ to OH. The mean power was 6.2 mW in the OH axis and 0.63 mW in the HO₂ axis throughout the campaign.

The precision was 0.03 pmol/mol (median) for OH and 0.42 pmol/mol for HO₂ at altitudes higher than 7 km. The limit of detection was calculated from the off-resonance measurement and determined to be 0.016 pmol/mol for OH and 0.33 pmol/mol for HO₂ in the upper troposphere for 1 minute average data.

b. Calibration

Calibrations were conducted before and after each flight, which started or ended at the airport in Hohn (Germany, 54° N, 9° E). The calibration method of the HORUS instrument is based on the method of Faloon et al. (2004) and described in more detail in Martinez et al. (2010).

As the calibration source, synthetic air (79 % N₂, 21 % O₂) was humidified and passed under a Hg Penray lamp. Photolysis of the gaseous water vapour produced OH and HO₂ (R 19 & 6, Table 1).

The theoretically produced concentrations of OH and HO₂ were calculated according to Equation 1:

$$[OH] = [HO_2] = \Phi_0 \sigma_{H_2O} [H_2O] t f_{O_2} \quad (1)$$

where σ is the absorption cross section of H₂O at 184.9 nm, [H₂O] is the water vapour concentration, t is irradiation time, f is a correction factor for the flux reduction due to absorption by O₂ throughout the height of the photolysis chamber, and Φ_0 is the photon flux of the Penray lamp which was determined by N₂O-actinometry (Figure 5). This method is described in more detail in Martinez et al. (2010).

The calculated OH and HO₂ concentrations were corrected for wall losses within the calibration system (6 % for OH and 2 % for HO₂) and then correlated with the measured fluorescence signal to obtain the instrument sensitivity, while potential OH and HO₂ loss at the wall surface within the instrument is considered through the calibration itself.

The detected fluorescence signal of the excited OH radicals at a given OH concentration depends mainly on laser power and internal pressure. The pressure determines the density and therefore the quantity of wall loss and the quenching efficiency of collisions between excited OH and N₂, O₂ and H₂O molecules, respectively. The internal density depends on the nozzle diameter at the inlet and on the ambient pressure, which changes with flight altitude.

Therefore, the ground-based calibration took into account this density dependency of the OH fluorescence signal. The internal pressure was changed by using different pinhole diameters during calibration. All ground-based calibrations were used to

calculate a global set of fit parameters. This set has been applied to fit the individual calibrations before and after each flight to determine the sensitivity for each pressure within the range of internal pressures experienced during the flight.

Figure 6 shows the density dependence of the mean sensitivity, C , observed during the calibration of the HOOVER summer campaign. The variability of the sensitivity with increasing pressure is a function of increasing density (due to an increasing OH concentration), decreasing wall loss and enhanced quenching (Faloona et al., 2004). The highlighted red area indicates the optimal internal pressure range of 2.5 to 5 mbar to be reached in the upper troposphere during the HOOVER flights.

In contrast to Martinez et al. (2010), a significant water dependency other than quenching was not observed during the calibrations. The OH concentration is calculated with the respective sensitivity, C , and the measured signal, S , as shown in Equation 2:

$$[OH] = \frac{S(OH)}{C(P, H_2O, T, \rho)} \quad (2)$$

c. Temperature dependent calibration

Due to its high reactivity, HO_x radicals could be lost within the detection system by wall contact. The design of the detection system consists of an inlet tube, a detection chamber to record the OH fluorescence signal, a spacer tube with an NO injector and a second detection chamber to record the “ HO_2 ” fluorescence signal. The sample is drawn through a nozzle into a reduced pressure detection system. Calculations of the velocity field show a compact jet between the inlet

nozzle and the detection chamber, indicating no wall contact of the air sample while transiting the inlet tube. However, the jet broadens and makes wall contact downstream of the first detection axis. Thus, OH and HO_2 losses can occur downstream of the first detection axis during measurement and calibration and are parameterised within the calibrated instrument sensitivity, with respect to pressure, density, and humidity variability. In order to characterize a potential temperature-dependent-sensitivity of HO_2 at low temperatures the inlet tube was wrapped in a cooling coil to simulate observed temperature profiles under laboratory conditions at constant OH and HO_2 mixing ratios. While the observed ambient temperatures had been between 256 and 223 K in the upper troposphere the internal temperature within the wing pod had not been lower than 253 K. During the temperature dependent calibration this observed internal temperature range and its temperature gradient were simulated.

Therefore, the distance between the winding of the cooling lines had been adapted to establish a temperature gradient similar to the one observed during flight. Under these conditions, a slightly higher signal (Figure 7) appeared at reduced temperatures in the OH axis. In contrast to this, the fluorescence signal of HO_2 significantly decreased in the second axis with decreasing temperature.

Since there is no evidence for a changing OH loss in the inlet tube the change of the OH signal is likely to be caused from cooling down the calibration unit or nearby electronics. Therefore, we corrected the elevated OH signal at reduced temperatures for both fluorescence signals of OH and HO_2 . Additionally, the HO_2

measurement was corrected accordingly to the lower fluorescence signal observed at reduced temperatures.

d. Interferences

Species which fluoresce at similar wavelengths as OH could interfere with the OH fluorescence measurement. By measuring the off-resonance signal at slightly larger and smaller wavelengths, the broad fluorescence signal of any potential interfering compounds or scatter from detection cell surfaces can be taken into account. The observed off-resonance signal was subtracted from the OH signal.

Possible interferences for our instrument have been studied e.g. during the HO_xComp campaign, a formal blind inter-comparison of six HO_x instruments (4 LIF, 1 DOAS (**D**ifferential **O**ptical **A**bsorption **S**pectroscopy) and 1 CIMS (**C**hemical **I**onisation **M**ass **S**pectroscopy)). Measurements were conducted in moderately polluted ambient air masses and under different conditions in the atmosphere simulation chamber SAPHIR in Jülich, Germany. The inter-comparison of the OH measurements performed with HORUS showed a linear correlation to the measurements of all five other instruments under day-light conditions (Schlosser et al., 2009). No unknown OH-interference was found for H₂O, O₃, NO_x, RO_x and several VOCs.

Mao et al. (2012) report experimental evidence that indicates an OH interference possibly from oxidation of VOC observed in a California forest within the planetary boundary layer. Also measurements using the HORUS system showed an OH interference during recent ground based field campaigns.

In contrast to observations within the planetary boundary layer, airborne side-by-side measurement of OH and HO₂ in the troposphere comparing a LIF-based instrument (ATHOS) and CIMS-technique shows in general reasonable agreement between the techniques (Ren et al. 2012). The combined measurement uncertainties are generally covering the differences indicating no additional OH interference.

In the paper of Baker et al. (2010) NMHCs observed in spring (Table 4) partly observed over Europe are highlighted. The observed levels of NMHCs would not introduce a significant OH reactivity or interference. Summertime observations obtained in 2007 from the CARIBIC project showed comparable NMHC mixing ratios in the upper troposphere over Europe compared to the published spring mixing ratios (personal communication: Angela Baker) and compare to published VOC mixing ratios obtained in northern mid-latitudes over continents (Jaegle et al. 2000).

Therefore, no OH interference in the upper troposphere over Europe is expected to affect the OH measurement significantly, even though the uncertainty of the OH measurement might be somewhat higher in convectively influenced air masses.

Fuchs et al. (2011) reports a HO₂ interference with RO₂ radicals for LIF instruments. This is stated to occur due to the NO injection into the air flow, which requires high NO mixing ratios up to more than 1000 µmol/mol, in order to quantitatively convert HO₂ into OH (R 12). Simultaneous production of HO₂ from RO₂ can lead to additional OH production via RO₂ (R 17 & 18). It was reported that the HO₂ yield is highest when the RO₂ is formed by reaction of OH with unsaturated

organic compounds. For small saturated hydrocarbons, the OH forming reactions of CH_3O_2 (< 5 %, (Holland et al., 2003)) and $\text{C}_2\text{H}_5\text{O}_2$ are negligible in the short reaction time between NO injection and OH detection.

The HOOVER measurements presented here were conducted in the upper troposphere. Thus, a considerable HO_2 interference impacting the measurement results is not likely, since ambient isoprene mixing ratios were lower than the limit of detection. Even in the air masses probed in the outflow region of the convective element no increased isoprene mixing ratios were observed. Assuming that oxidation of NMHCs (Non Methane HydroCarbons) during the convective transport formed RO_2 radicals, the uncertainty of the observed HO_2 mixing ratios can be somewhat higher due to a potential RO_2 interference.

In agreement with this the global model mixing ratios of NMHCs were negligible; e. g. the median upper tropospheric mixing ratio of isoprene was $1.86 \cdot 10^{-16}$ mol/mol along the HOOVER flight trajectory. However, no NMHCs have been applied to the box model either. The results of the constrained box model simulations reproduce the OH and HO_2 concentrations indicating that the important HO_x chemistry is covered. Therefore differences between the model results and their comparison to the observations are apparently not likely to be caused by the negligible NMHC concentrations within the global model.

4. Box model CAABA/MECCA

a. Description

We used the atmospheric chemistry box model CAABA/MECCA-2.7b (Chemistry

As A Boxmodel Application/Module Efficiently Calculating the Chemistry of the Atmosphere). The parts of the model that were used for this study do not differ substantially from version 3.0 described by Sander et al. (2011a). To connect the box model CAABA to the MECCA chemistry module and to physical processes, we used the MESSy (Modular Earth Submodel System) interface by Jöckel et al. (2005). MESSy formally describes a way to connect different process and diagnostic submodels to a more comprehensive model system. The key ideas are the modular, object oriented approach, and the strict separation between model infrastructure (such as data exchange, input/output, memory management etc.) from the actual scientific content (e.g. the parameterisations, numerical solvers, etc.) into 4 different software layers. Information about the implementation of the recent (2nd generation) MESSy infrastructure have been documented by Jöckel et al. (2010). The model simulations were executed in multi-simulation and steady-state mode, see Sander et al. (2011a) for details. Thus, multiple model simulations were performed, and each model simulation continued until the relative changes of OH and HO_2 according to equation (4) were less than 10^{-6} within a 15 minute time step:

$$\left| \frac{\Delta[\text{OH}]}{[\text{OH}]} \right| = \frac{[\text{OH}(t + \Delta t)] - [\text{OH}(t)]}{[\text{OH}(t)]} \leq 10^{-6} \quad (3)$$

Measured values were split into data sets for 60 s time intervals, and one model simulation was performed for each data set. The model simulations were constrained by fixing the measured species (NO , CO , O_3 , H_2O , H_2O_2 , sum of ROOH as CH_3OOH , and CH_4) to their observed

values. H_2 was fixed to $0.6 \mu\text{mol/mol}$, and CH_4 to $1.8 \mu\text{mol/mol}$ when not measured. From the comprehensive chemical reaction mechanism (Sander et al., 2011a), we have selected the basic O_3 , NO_x , HO_x , and CH_4 chemistry. Reactions of higher hydrocarbons ($\geq C_2$), halogens, and sulphur compounds were switched off for our model simulation. The simple HO_x -budget scheme, which is expected to dominate HO_x production and loss in the constrained box model under upper tropospheric conditions, is summarized in Table 1. As mentioned previously, rather low mixing ratios of NMHCs were computed by the global model. In comparison to global model simulations, neglecting the OH reactivity due to reactions with NMHCs should not influence the box model results significantly.

Photolysis frequencies, which were needed as model input, were calculated with the radiative transfer model TUV (Tropospheric Ultraviolet-Visible model V 4.1) (Madronich and Flocke, 1998) along the flight trajectories. As Palancar et al. (2011) stated, the TUV model is able to reproduce an observed actinic flux under cloud free conditions (1.01 ± 0.04). A comparison of all obtained observations to cloud-free model results showed an enlarged uncertainty of the model results (1.1 ± 0.3).

To minimize cloud effects, we used measured $J(NO_2)$ to scale the calculated values for cloud effects as described in Stickler et al. (2006).

CAABA simulations were performed for the northbound flights from southern Germany ($48^\circ N$) to northern Scandinavia ($68^\circ N$) only since NO and CO

measurements were not available during the southbound flights.

b. Monte-Carlo simulations

The Monte-Carlo method was used to estimate the uncertainty of simulated OH and HO_2 values as a result of uncertainties in the values of the chemical rate coefficients. Each Monte-Carlo simulation encompasses a set of 9999 individual model simulations. For each of these model simulations, all rate coefficients were multiplied with randomly chosen factors. These factors are scaled with the uncertainties of the rate coefficients (taken from the IUPAC and JPL recommendations (Atkinson et al., 2007; S. Sander et al., 2011b)) and are centered around 1.

Results of one Monte-Carlo-simulation of OH and HO_2 are given in Figure 8. The calculated median and percentiles of OH and HO_2 were $0.304^{+0.02}_{-0.05}$ pmol/mol and $21.0^{+1.0}_{-2.3}$ pmol/mol, respectively. The percentiles at 31.7 % and 68.3 % of the distribution were used as an estimate of the 1σ -uncertainty.

c. Results

CAABA reproduces the observed OH and HO_2 mixing ratios reasonably well. Figure 9 a, b shows that more than 98 % of the calculated OH mixing ratios are scattered within a range of ± 0.3 pmol/mol around the observed values. The scatter of the calculated HO_2 mixing ratios is somewhat higher. The error bars shown in Figure 9 a, b indicate the uncertainties of the measured values (horizontal) and the Monte-Carlo-simulations (vertical), the latter being due to the uncertainty of the rate coefficients.

The number distribution of the calculated quotients of simulated and observed OH

mixing ratios result in an asymmetric (skew) distribution with an arithmetic mean value around 1. Since there are no negative values allowed for both of the number distributions half of the calculated distribution is projected to the interval [0,1], whereas the remaining part is projected to [1,+inf] causing the log-normal distribution.

The box model underestimates the observed OH and HO₂ mixing ratios marginally, since the slope of the fit in Figure 9 a, b, the maximum of the probability distribution and the maximum of the fitted log-normal distribution are all slightly smaller than 1 for OH and HO₂. The median underestimation is 1.8 % for OH and 3.7 % for HO₂, typically within the uncertainty of the measurements and of the rate constants used.

d. Comparison to previous campaigns

Ren et al. (2008) compared observed and (box model) simulated OH and HO₂ mixing ratios of three airborne campaigns. Two of these campaigns were performed in mid-latitudes. In summer 2004 INTEX-(N)A was carried out over Northern America and the western Atlantic Ocean (Singh et al., 2006). In spring 2001 TRACE-P was conducted over the northern Pacific region (Jacob et al., 2003). PEM-(T)B was performed in spring 1999 in the tropical Pacific area (Browell et al., 2001).

The study of Ren et al. (2008) reports that a constrained box model reproduces the observed OH mixing ratios with good agreement for all three campaigns. Also the observed HO₂ mixing ratios were comparable to the model calculations of the TRACE-P and PEM-(T)B campaign.

During the INTEX-(N)A campaign a higher load of pollutants was observed in the air masses of the upper troposphere compared to TRACE-P and PEM-(T)B. Thus, the model tended to underestimate HO₂ up to a factor of more than 3 (median values of altitude bins) under those upper tropospheric conditions. The planetary boundary layer and mid troposphere HO₂ mixing ratios are generally satisfactorily reproduced by the box model, while starting at an altitude of 8 km HO₂ is underestimated, with an increasing trend until 11 km height.

The observed HO₂ mixing ratios during INTEX-(N)A were roughly between 10 pmol/mol and 30 pmol/mol and are comparable to the HOOVER observations of HO₂ mixing ratios of about 5 pmol/mol to 30 pmol/mol. With increasing altitude a decreasing trend of HO₂ mixing ratios was found for both campaigns.

The observed-to-calculated comparison for the INTEX-(N)A campaign showed that the box model used to reproduce the observed OH mixing ratios in the upper troposphere produced good agreement. The same result is found for the comparison between the HOOVER OH observation and box model simulation. While Ren et al. (2008) report OH mixing ratios between 0.1 pmol/mol and 0.8 pmol/mol, a larger range of OH mixing ratios of up to 3 pmol/mol was observed in the upper troposphere during the HOOVER campaign. A similar trend of increasing OH mixing ratios with altitude was observed during both campaigns. For INTEX-(N)A 0.3 pmol/mol (median value) OH at 7 km and 0.7 pmol/mol OH at 11 km were reported. During the HOVER campaign median OH mixing ratios were

between 0.3 pmol/mol at 7 km and 1 pmol/mol at 11 km.

In contrast to Ren et al. (2008), we did not observe an offset between the measured and the box model simulated HO₂ mixing ratios. We find a good agreement between observations and calculations, indicating no major lack of understanding of the chemistry under the probed background conditions. During HOOVER 2 in the upper troposphere observed OH mixing ratios are on average comparable to those observed during INTEX-(N)A and higher than the observed OH mixing ratios of the PEM-(T)B, and TRACE-P campaigns. However, OH mixing ratios observed under NO_x levels higher than 50 pmol/mol exceed the observed OH mixing ratios of the respective campaigns. Observed HO₂ mixing ratios exceed the INTEX-(N)A, PEM-(T)B and TRACE-P observations.

With regard to CO, NO and ozone, the conditions observed during HOOVER 2 are more comparable to INTEX-(N)A, while the higher OH mixing ratios found are likely due to a higher HO₂ conversion rate caused by enhanced NO mixing ratios observed in convectively affected air masses in the upper troposphere over Europe (Olson et al., 2006; Olson et al., 2004; Ren et al., 2008; Tan et al., 2001).

5. General circulation model EMAC

a. Description

EMAC (ECHAM5 version 5.3.02/MESSy version 2.41 Atmospheric Chemistry) is based on the general circulation model ECHAM5 (ECMWF, Hamburg, Version 5, (Roeckner et al., 2006)), which is coupled to the Modular Earth Submodel System (MESSy (Jöckel et al., 2010)). The chemistry scheme is MECCA as also used in CAABA/MECCA box model

simulations. However, in the 3D simulation analysed here, the initialized number of trace gas species is much larger and includes NMHC species compared to the box model and the species concentrations are not constrained by measurements. A description of the applied emission inventory is given in Jöckel et al. (2010).

The submodels ONLEM, OFFLEM, TNUDGE and DRYDEP were applied to calculate primary emissions and dry deposition of trace gases and aerosols (Kerkweg et al., 2006a; Kerkweg et al., 2006b). Wet scavenging on cloud particles and aqueous-phase chemistry in cloud droplets were simulated with the submodel SCAV (Tost et al., 2006).

EMAC was applied in the T42L90MA-resolution, i.e. with a spherical truncation of T42 (corresponding to a quadratic Gaussian grid of approx. 2.8 by 2.8 degrees in latitude and longitude) with 90 vertical hybrid pressure levels up to 0.01 hPa.

In order to fly “virtually” through the grid boxes of the global numerical chemistry and climate simulation system the S4D submodel was used (Jöckel et al., 2010). It performs a bi-linear interpolation of the model results in space and time along the flight track positions.

$$FTT \subset MT \pm \frac{\Delta t}{2} \quad (4)$$

For each time interval, S4D searches for the corresponding measurement point along the flight track according to equation 4. Whenever a flight track time point (FTT) is within half of the model time step ($\Delta t/2$) around the model time (MT) the submodel performs two horizontal interpolations using the 4 closest grid

points at two model levels (above and below the flight track), and then a linear interpolation in the vertical to the flight track. The result is written into an output file.

This method provides a model calculated value of all tracers and reaction rates along the flight track with a time resolution of the model time step (12 minutes in this analysed simulation).

b. Results

In general, EMAC significantly underestimates the observed OH and HO₂ mixing ratios (Figure 9 c, d) in the upper troposphere. Most of the simulated OH values are scattered around the observed ones within a range of ± 0.3 pmol/mol, as also perceived from the CAABA simulation. However, the fraction (75 %) of simulated values within the range is substantially smaller compared to the CAABA calculations (98 %). Furthermore, the EMAC model systematically underestimates OH and HO₂ (Figure 9 c, d). 67 % of the calculated OH values and 94 % of the calculated HO₂ values are smaller than the observed. The median underestimation of OH and HO₂ compared to the observations is 24 % and 41 %, respectively.

The comparison of EMAC simulated and observed OH and HO₂ mixing ratios also show a log-normal like distribution. The log-normal like distribution is found because there are no negative values allowed for both of the number distributions. As previously described for CAABA, half of the calculated distribution is projected to the interval [0,1], whereas the remaining part is projected to [1,+inf]. However, in contrast to the CAABA results this number distribution is shifted

towards a large underestimation of OH and HO₂.

Since both models utilize a similar chemical mechanism the underestimation of both species by the global model indicates that (1) precursor mixing ratios and (2) possibly reaction and photolysis rates are less well reproduced within the unconstrained 3D-model, because the global model is not constrained to changes of meteorological parameters such as temperature, pressure or enhanced photolysis frequencies closely above clouds. Furthermore, the 3D model simulates additional processes not represented by the box model, such as large-scale, convective, and diffusive tracer transport and wet-scavenging of soluble constituents. Small-scale processes like convective transport cannot be resolved by large-scale models leading to over and underestimations of trace gases in the plumes.

A comparison of the observed and simulated OH and HO₂ mixing ratios (Figures 9 - 11) and the two computed HO_x-budgets highlights several differences in the OH-budget, which directly affect the calculated OH mixing ratios. In the following comparison between observation and the global 3D-model output, we focus on the impact of hydrogen peroxide as a primary OH source, the impact of CO and NO on the HO_x-equilibrium and the influence of convective transport on the HO_x-budget comparison.

Influence of H₂O₂

In Figure 10 a) the blue ellipse highlights that the EMAC model tends to underestimate the observed OH mixing ratios most strongly when the H₂O₂ mixing ratio is strongly underestimated compared to the observations.

This under prediction of OH is not always directly linked to the quality of the H₂O₂ reproduction within the global model. The red ellipse in Figure 10 a) highlights data when the model reproduces the OH even though the H₂O₂ is clearly underestimated (blue arrow). In contrast, for other points for which H₂O₂ mixing ratios are well reproduced by the model the OH is underestimated (red arrow).

Figure 10 b) shows that when the OH is well reproduced despite underestimated H₂O₂ mixing ratios, NO mixing ratios are simultaneously overestimated (red arrow in subplot b). Apparently, the underrated OH source from H₂O₂-photolysis is compensated in the model by a stronger OH source from reactions of NO. When OH is underestimated despite well reproduced H₂O₂, NO mixing ratios are underestimated (blue arrow) leading to a too low OH formation from this source.

HO₂ is almost always underestimated even if the H₂O₂ is well reproduced by the model, as seen in Figure 9 d. A clear correlation links the lowest and the most underestimated HO₂ mixing ratio to the level of H₂O₂ underestimation. Coupled convective transport of H₂O₂ and NO_x and local NO_x formation by lightning might lead to an underestimation of H₂O₂ and NO_x in the convectively influenced air masses within the upper troposphere. Therefore, an underestimation of simulated OH can be promoted from an underestimated HO₂ conversion into OH.

OH production rate by H₂O₂ photolysis

Since the OH forming reaction of O(¹D) weakens with altitude, due to lower water content of the air masses, other OH producing pathways like photolysis of H₂O₂ and HCHO become more important (Tan et al., 2001).

It was shown above in Figure 9 c, d, that H₂O₂ is underestimated by the model. This leads to a too small primary OH source through H₂O₂ photolysis. The colour coding of Figure 11 e-h gives the relative importance of the H₂O₂ dependent OH source in relation to the strength of the O(¹D) dependent OH source. These figures combined clearly highlight that the OH underestimation by the model simulations is due to the underestimated H₂O₂ mixing ratios, which gives rise to a primary OH production rate for the outlying dots of the southern leg which is too small (see blue rectangle in Figure 11 g).

A more complex situation is found in the highlighted area shown in Figure 11 e. Here, the slight underestimation of OH might be explained by the H₂O₂ mixing ratio, since the H₂O₂ dependent OH production rate is an important contributor to the overall primary OH production. However, no correlation to the degree of H₂O₂ underestimation could be found (Figure 10 a). Figure 10 b indicates in the same area a correlation between the degree of OH underestimation and the underestimation of NO, since OH is the better reproduced at higher NO ratios (modelled to observed) and the lower the H₂O₂ ratios. In contrast to the data shown in the blue ellipse (same Figures), here OH is underestimated when the model reproduces the H₂O₂. Thus, a missing HO₂ conversion rate is likely responsible for the OH underestimation.

The comparison of observed and simulated HO₂ shows a correlation between the degree of HO₂ underestimation and the missing H₂O₂ (Figure 9 d) as well as the importance of the H₂O₂ dependent OH source (Figure 11 f, h) for the OH.

A high OH mixing ratio of 3.25 pmol/mol was observed in the outflow region of a convective system over Germany. The upper tropospheric composition was in this case affected by fresh convective outflow, not resolved by the global model, which parameterises these small-scale processes. Nevertheless, these observations give an indication of how the mixing ratios of different tracers in the EMAC model can be related to air masses within the outflow region of a small-scale convective regime.

Influence of convective transport

For the southern flight tracks NO and CO measurements were not available. Therefore, the ratio between H₂O₂ and organic peroxides (referred as ROOH) was taken as a proxy for convective transport. Even though identifying convectively influenced air masses by the peroxide ratio has a larger uncertainty than identifying convective influence through other trace gas mixing ratios convectively influenced air masses were identified using the ratio of H₂O₂ to CH₃OOH (based on (Snow et al., 2007) and references therein). In our study, enhanced H₂O₂ mixing ratios were typically found in convectively affected air masses. Nevertheless, the H₂O₂/ROOH ratio was reduced, since ROOH was even more strongly enhanced and less scavenged through the aqueous phase removal and rainout. A more detailed discussion will be presented in Bozem et al. (in preparation).

Small peroxide ratios indicate influences of convection on the trace gas distribution whenever the OH and HO₂ underestimation is prominent on the southern flight tracks (Figure 9 g,h). As indicated by the OH/HO₂ ratio (Figure 11 c), along with peroxides NO_x was convectively injected into the upper

troposphere shifting the HO_x equilibrium towards the OH. Underprediction of HO₂ than results in an promoted OH underestimation, since a primary OH source (photolysis of H₂O₂) and HO₂ cycling (with NO) into OH is underestimated.

The observed OH and HO₂ mixing ratios of the northern flight tracks do not appear to be much affected by convective transport.

HO_x-equilibrium

The HO_x-equilibrium is mainly influenced by NO and CO (R 12 & 14), which inter-convert the two species (Jaegle et al., 2001). The HO_x sum is virtually always underestimated by the global model. An underestimation of CO and a mostly overestimated NO reproduces the OH relatively well, while HO₂ is strongly underestimated (see Figure 10 b, red ellipse). HO₂ is reproduced best when the CO-ratio (simulated/measured not shown) is close to 1 and calculated OH cycling rates into HO₂ are close to realistic values.

OH/HO₂ratio

The variability of the OH/HO₂-ratio is mainly influenced by the NO-variability (Ren et al., 2008), which is usually higher than the CO-variability. During background conditions as observed during the HOOVER summer flights shown here, the mean CO mixing ratio was 97.5 nmol/mol, with a standard deviation of 15 % and the NO mean value was 57.5 pmol/mol with a standard deviation of 99 %. Other studies (Jaegle et al., 2001; Martinez et al., 2003; Ren et al., 2008) report the same NO related OH/HO₂-behaviour. Accordingly, the OH/HO₂-ratio can be used to display relative changes of the HO₂-conversion rate due to changes in NO.

The colour coding in Figure 11 a-d displays increasing OH mixing ratios with an increasing OH/HO₂-ratio along the northern flight leg and an increasing OH underestimation along the southbound flight leg. In both regions, smaller HO₂ mixing ratios are found during high OH/HO₂-ratios and no correlation to the level of underestimation of HO₂ is observed.

Comparison to previous model studies

HO_x observations from the ATHOS instrument were compared to results of GEOS-Chem simulations indicating that the HO_x budget is not entirely resolved by the global model. For the INTEX-(N)A campaign an OH and HO₂ overestimation of 60 % and 30 %, respectively, were reported for higher altitudes (Hudman 2007). A later recalibration of the ATHOS instrument revised OH and HO₂ mixing ratios to be a factor of 1.64 higher (Ren et al. 2008). Since the global model then tends to underestimate HO₂, the HO₂ and HO_x budget remains uncovered. Zhang et al. (2008) report that the same global model reproduces the HO₂ observations obtained during the INTEX-B campaign but overestimates OH by 27 %. A comparison of observed HO_x mixing ratios observed during the ARCTAS campaign to the global model found overestimated HO₂, speculatively caused by underestimated uptake of HO₂ on aerosols (Mao 2010).

6. Summary and Conclusion

The HO_x measurements performed during the HOOVER summer campaign show unexpectedly high OH mixing ratios up to more than 3 pmol/mol and HO₂ mixing ratios up to more than 25 pmol/mol in the upper troposphere over central and

northern Europe. The comparison of the measurements to the box model CAABA/MECCA calculated mixing ratios reveal excellent agreement between calculations and observations. These calculations were done with a simple chemical mechanism, constrained by the measurements, indicating no major lack of understanding of the chemistry under the probed background conditions. The comparison to the global 3D circulation model EMAC (executed with a similar chemical mechanism as used for the constrained CAABA calculations) shows a substantial and systematic underestimation of the observed OH and HO₂ mixing ratios. This underestimation of the HO_x mixing ratios is caused by underestimated HO_x precursor mixing ratios, in particular H₂O₂, related to the treatment of this gas in the transport and deposition routines. The study of Klippel et al. (2011) indicates that the global model fails to reproduce H₂O₂ since micro-physical processes of wet scavenging of soluble trace gas species is neither fully understood nor well parameterized within the global model. Since H₂O₂ can be an important upper tropospheric primary source of OH, the global model consistently underestimates the OH mixing ratio when underestimating the H₂O₂.

The model tends to underestimate not only H₂O₂ but also NO mixing ratios in convectively transported air masses. The consequences are an overall too low simulated HO_x level and underestimated simulated OH mixing ratios. For the southern flight tracks NO and CO measurements were not available. As indicated by the OH/HO₂ ratio, along with peroxides NO_x was convectively injected into the upper troposphere shifting the HO_x

equilibrium towards the OH. Underprediction of HO₂ than results in a stronger OH underestimation, since a primary OH source (photolysis of H₂O₂) as well as HO₂ cycling (with NO) into OH is underestimated.

Apparently, in the case of a NO overestimation the too high HO₂ conversion rates can balance the underestimated H₂O₂ photolysis rates and the simulated OH is in agreement with the observations. In this case, the HO_x-budget is not represented within the model and OH is reproduced through incorrect source strengths. However, further observations and comparisons are needed to investigate the significance of this finding.

As other studies have shown, it is a challenge for global models to calculate the transport of highly soluble trace gases like H₂O₂ and HCHO (Klippel et al., 2011; Tost et al., 2006). Models refined to solve small-scale process are needed to investigate convective transport processes and scavenging of soluble trace species, as well as in cloud chemistry and the rejection of peroxides during freezing (Lelieveld and Crutzen, 1990; Mari et al., 2000).

We have shown that the uncertainties related to these processes lead to substantial ambiguity in the model calculated oxidation capacity of the upper troposphere.

Acknowledgements. The authors are very grateful to the HOOVER team, Enviscope GmbH and the Gesellschaft für Flugziieldarstellung (GFD) for their great support. Their work was instrumental for the HOOVER project.

The service charges for this open access publication have been covered by the Max Planck Society.

Literature

Atkinson, R., Baulch, D. L., Cox, R. A., Crowley, J. N., Hampson, R. F., Hynes, R. G., Jenkin, M. E., Rossi, M. J., and Troe, J.: Evaluated kinetic and

photochemical data for atmospheric chemistry: Volume III - gas phase reactions of inorganic halogens, *Atmos Chem Phys*, 7, 981-1191, 2007.

Baker, A. K., Slemr, F., and Brenninkmeijer, C. A. M.: Analysis of non-methane hydrocarbons in air samples collected aboard the CARIBIC passenger aircraft, *Atmos Meas Tech*, 3, 311-321, 2010.

Barth, M. C., Stuart, A. L., and Skamarock, W. C.: Numerical simulations of the July 10, 1996, Stratospheric-Tropospheric Experiment: Radiation, Aerosols, and Ozone (STERA0)-Deep Convection experiment storm: Redistribution of soluble tracers, *J Geophys Res-Atmos*, 106, 12381-12400, 2001.

Beygi, Z. H., Fischer, H., Harder, H. D., Martinez, M., Sander, R., Williams, J., Brookes, D. M., Monks, P. S., and Lelieveld, J.: Oxidation photochemistry in the Southern Atlantic boundary layer: unexpected deviations of photochemical steady state, *Atmos Chem Phys*, 11, 8497-8513, DOI 10.5194/acp-11-8497-2011, 2011.

Bozem, H., Fischer, H., Schiller, C. L., Klippel, T., Koenigstedt, R., Parchatka, U., Custer, T., Williams, J., Regelin, E., Harder, H., Martinez, M., Smoydzin, L., Lawrence, M. G., Wernli, H., Zimmer, M., Sander, R., and Lelieveld, J.: The influence of deep convection on formaldehyde and hydrogen peroxide in the upper troposphere over Europe in preparation.

Browell, E. V., Fenn, M. A., Butler, C. F., Grant, W. B., Ismail, S., Ferrare, R. A., Kooi, S. A., Brackett, V. G., Clayton, M. B., Avery, M. A., Barrick, J. D. W., Fuelberg, H. E., Maloney, J. C., Newell, R. E., Zhu, Y., Mahoney, M. J., Anderson, B. E., Blake, D. R., Brune, W. H., Heikes, B. G., Sachse, G. W., Singh, H. B., and Talbot, R. W.: Large-scale air mass characteristics observed over the remote tropical Pacific Ocean during March-April 1999: Results from PEM-Tropics B field experiment, *J Geophys Res-Atmos*, 106, 32481-32501, 2001.

Faloona, I. C., Tan, D., Leshner, R. L., Hazen, N. L., Frame, C. L., Simpas, J. B., Harder, H., Martinez, M., Di Carlo, P., Ren, X. R., and Brune, W. H.: A laser-induced fluorescence instrument for detecting tropospheric OH and HO₂: Characteristics and calibration, *J Atmos Chem*, 47, 139-167, 2004.

Fuchs, H., Bohn, B., Hofzumahaus, A., Holland, F., Lu, K. D., Nehr, S., Rohrer, F., and Wahner, A.: Detection of HO(2) by laser-induced fluorescence: calibration and interferences from RO(2) radicals, *Atmos Meas Tech*, 4, 1209-1225, DOI 10.5194/amt-4-1209-2011, 2011.

- Holland, F., Hofzumahaus, A., Schafer, R., Kraus, A., and Patz, H. W.: Measurements of OH and HO(2) radical concentrations and photolysis frequencies during BERLIOZ, *J Geophys Res-Atmos*, 108, Artn 8246, Doi 10.1029/2001jd001393, 2003.
- Hudman, R. C., Jacob, D. J., Turquety, S., Leibensperger, E. M., Murray, L. T., Wu, S., Gilliland, A. B., Avery, M., Bertram, T. H., Brune, W., Cohen, R. C., Dibb, J. E., Flocke, F. M., Fried, A., Holloway, J., Neuman, J. A., Orville, R., Perring, A., Ren, X., Sachse, G. W., Singh, H. B., Swanson, A., and Wooldridge, P. J.: Surface and lightning sources of nitrogen oxides over the United States: Magnitudes, chemical evolution, and outflow, *J Geophys Res-Atmos*, 112, Artn D12s05, Doi 10.1029/2006jd007912, 2007.
- Jacob, D. J., Crawford, J. H., Kleb, M. M., Connors, V. S., Bendura, R. J., Raper, J. L., Sachse, G. W., Gille, J. C., Emmons, L., and Heald, C. L.: Transport and Chemical Evolution over the Pacific (TRACE-P) aircraft mission: Design, execution, and first results, *J Geophys Res-Atmos*, 108, 1-19, Artn 9000, Doi 10.1029/2002jd003276, 2003.
- Jaegle, L., Jacob, D. J., Brune, W. H., Faloona, I., Tan, D., Heikes, B. G., Kondo, Y., Sachse, G. W., Anderson, B., Gregory, G. L., Singh, H. B., Pueschel, R., Ferry, G., Blake, D. R., and Shetter, R. E.: Photochemistry of HOx in the upper troposphere at northern midlatitudes, *J Geophys Res-Atmos*, 105, 3877-3892, 2000.
- Jaegle, L., Jacob, D. J., Brune, W. H., and Wennberg, P. O.: Chemistry of HOx radicals in the upper troposphere, *Atmos Environ*, 35, 469-489, 2001.
- Jöckel, P., Sander, R., Kerkweg, A., Tost, H., and Lelieveld, J.: Technical note: The Modular Earth Submodel System (MESSy) - a new approach towards Earth System Modeling, *Atmos Chem Phys*, 5, 433-444, 2005.
- Jöckel, P., Kerkweg, A., Pozzer, A., Sander, R., Tost, H., Riede, H., Baumgaertner, A., Gromov, S., and Kern, B.: Development cycle 2 of the Modular Earth Submodel System (MESSy2), *Geosci Model Dev*, 3, 717-752, DOI 10.5194/gmd-3-717-2010, 2010.
- Kerkweg, A., Buchholz, J., Ganzeveld, L., Pozzer, A., Tost, H., and Jockel, P.: Technical note: An implementation of the dry removal processes DRY DEPosition and SEDImentation in the modular earth submodel system (MESSy), *Atmos Chem Phys*, 6, 4617-4632, 2006a.
- Kerkweg, A., Sander, R., Tost, H., and Jockel, P.: Technical note: Implementation of prescribed (OFFLEM), calculated (ONLEM), and pseudo-emissions (TNUDGE) of chemical species in the Modular Earth Submodel System (MESSy), *Atmos Chem Phys*, 6, 3603-3609, 2006b.
- Klippel, T., Fischer, H., Bozem, H., Lawrence, M. G., Butler, T., Jockel, P., Tost, H., Martinez, M., Harder, H., Regelin, E., Sander, R., Schiller, C. L., Stickler, A., and Lelieveld, J.: Distribution of hydrogen peroxide and formaldehyde over Central Europe during the HOOVER project, *Atmos Chem Phys*, 11, 4391-4410, DOI 10.5194/acp-11-4391-2011, 2011.
- Lelieveld, J., and Crutzen, P. J.: Influences of Cloud Photochemical Processes on Tropospheric Ozone, *Nature*, 343, 227-233, 1990.
- Levy, H.: Normal Atmosphere - Large Radical and Formaldehyde Concentrations Predicted, *Science*, 173, 141-143, 1971.
- Madronich, S., and Flocke, S.: The role of solar radiation in atmospheric chemistry, in: *Handbook of Environmental Chemistry, Handbook of Environmental Chemistry*, Springer, New York, 1-26, 1998.
- Mao, J., Jacob, D. J., Evans, M. J., Olson, J. R., Ren, X., Brune, W. H., St Clair, J. M., Crouse, J. D., Spencer, K. M., Beaver, M. R., Wennberg, P. O., Cubison, M. J., Jimenez, J. L., Fried, A., Weibring, P., Walega, J. G., Hall, S. R., Weinheimer, A. J., Cohen, R. C., Chen, G., Crawford, J. H., McNaughton, C., Clarke, A. D., Jaegle, L., Fisher, J. A., Yantosca, R. M., Le Sager, P., and Carouge, C.: Chemistry of hydrogen oxide radicals (HOx) in the Arctic troposphere in spring, *Atmos Chem Phys*, 10, 5823-5838, DOI 10.5194/acp-10-5823-2010, 2010.
- Mao, J., Ren, X., Zhang, L., Van Duin, D. M., Cohen, R. C., Park, J. H., Goldstein, A. H., Paulot, F., Beaver, M. R., Crouse, J. D., Wennberg, P. O., DiGangi, J. P., Henry, S. B., Keutsch, F. N., Park, C., Schade, G. W., Wolfe, G. M., Thornton, J. A., and Brune, W. H.: Insights into hydroxyl measurements and atmospheric oxidation in a California forest, *Atmos Chem Phys*, 12, 8009-8020, DOI 10.5194/acp-12-8009-2012, 2012.
- Mari, C., Jacob, D. J., and Bechtold, P.: Transport and scavenging of soluble gases in a deep convective cloud, *J Geophys Res-Atmos*, 105, 22255-22267, 2000.
- Mari, C., Saut, C., Jacob, D. J., Staudt, A., Avery, M. A., Brune, W. H., Faloona, I., Heikes, B. G., Sachse, G. W., Sandholm, S. T., Singh, H. B., and

- Tan, D.: On the relative role of convection, chemistry, and transport over the South Pacific Convergence Zone during PEM-Tropics B: A case study, *J Geophys Res-Atmos*, 108, Artn 8232, DOI 10.1029/2001jd001466, 2002.
- Martinez, M., Harder, H., Kovacs, T. A., Simpas, J. B., Bassis, J., Leshner, R., Brune, W. H., Frost, G. J., Williams, E. J., Stroud, C. A., Jobson, B. T., Roberts, J. M., Hall, S. R., Shetter, R. E., Wert, B., Fried, A., Alicke, B., Stutz, J., Young, V. L., White, A. B., and Zamora, R. J.: OH and HO(2) concentrations, sources, and loss rates during the Southern Oxidants Study in Nashville, Tennessee, summer 1999, *J Geophys Res-Atmos*, 108, Artn 4617, DOI 10.1029/2003jd003551, 2003.
- Martinez, M., Harder, H., Kubistin, D., Rudolf, M., Bozem, H., Eerdeken, G., Fischer, H., Klupfel, T., Gurk, C., Konigstedt, R., Parchatka, U., Schiller, C. L., Stickler, A., Williams, J., and Lelieveld, J.: Hydroxyl radicals in the tropical troposphere over the Suriname rainforest: airborne measurements, *Atmos Chem Phys*, 10, 3759-3773, 2010.
- Olson, J. R., Crawford, J. H., Chen, G., Fried, A., Evans, M. J., Jordan, C. E., Sandholm, S. T., Davis, D. D., Anderson, B. E., Avery, M. A., Barrick, J. D., Blake, D. R., Brune, W. H., Eisele, F. L., Flocke, F., Harder, H., Jacob, D. J., Kondo, Y., Lefer, B. L., Martinez, M., Mauldin, R. L., Sachse, G. W., Shetter, R. E., Singh, H. B., Talbot, R. W., and Tan, D.: Testing fast photochemical theory during TRACE-P based on measurements of OH, HO(2), and CH(2)O, *J Geophys Res-Atmos*, 109, Artn D15s10, DOI 10.1029/2003jd004278, 2004.
- Olson, J. R., Crawford, J. H., Chen, G., Brune, W. H., Faloon, I. C., Tan, D., Harder, H., and Martinez, M.: A reevaluation of airborne HOx observations from NASA field campaigns, *J Geophys Res-Atmos*, 111, Artn D10301, DOI 10.1029/2005jd006617, 2006.
- Palancar, G. G., Shetter, R. E., Hall, S. R., Toselli, B. M., and Madronich, S.: Ultraviolet actinic flux in clear and cloudy atmospheres: model calculations and aircraft-based measurements, *Atmos Chem Phys*, 11, 5457-5469, DOI 10.5194/acp-11-5457-2011, 2011.
- Prather, M. J., and Jacob, D. J.: A persistent imbalance in HOx and NOx photochemistry of the upper troposphere driven by deep tropical convection, *Geophys Res Lett*, 24, 3189-3192, 1997.
- Ren, X., Mao, J., Brune, W. H., Cantrell, C. A., Mauldin, R. L., Hornbrook, R. S., Kosciuch, E., Olson, J. R., Crawford, J. H., Chen, G., and Singh, H. B.: Airborne intercomparison of HOx measurements using laser-induced fluorescence and chemical ionization mass spectrometry during ARCTAS, *Atmos Meas Tech*, 5, 2025-2037, DOI 10.5194/amt-5-2025-2012, 2012.
- Ren, X. R., Olson, J. R., Crawford, J. H., Brune, W. H., Mao, J. Q., Long, R. B., Chen, Z., Chen, G., Avery, M. A., Sachse, G. W., Barrick, J. D., Diskin, G. S., Huey, L. G., Fried, A., Cohen, R. C., Heikes, B., Wennberg, P. O., Singh, H. B., Blake, D. R., and Shetter, R. E.: HO(x) chemistry during INTEX-A 2004: Observation, model calculation, and comparison with previous studies, *J Geophys Res-Atmos*, 113, Artn D05310, DOI 10.1029/2007jd009166, 2008.
- Roeckner, E., Brokopf, R., Esch, M., Giorgetta, M., Hagemann, S., Kornblueh, L., Manzini, E., Schlese, U., and Schulzweida, U.: Sensitivity of simulated climate to horizontal and vertical resolution in the ECHAM5 atmosphere model, *J Climate*, 19, 3771-3791, 2006.
- Sander, R., Baumgaertner, A., Gromov, S., Harder, H., Jockel, P., Kerkweg, A., Kubistin, D., Regelin, E., Riede, H., Sandu, A., Taraborrelli, D., Tost, H., and Xie, Z. Q.: The atmospheric chemistry box model CAABA/MECCA-3.0, *Geosci Model Dev*, 4, 373-380, DOI 10.5194/gmd-4-373-2011, 2011a.
- Sander, S. P., Abbatt, J., Barker, J. R., Burkholder, J. B., Friedl, R. R., Golden, D. M., Huie, R. E., Kolb, C. E., Kurylo, M. J., Moortgat, G. K., Orkin, V. L., and Wine, P. H.: Chemical Kinetics and Photochemical Data for Use in Atmospheric Studies, Evaluation No. 17, JPL Publication 10-6, Jet Propulsion Laboratory, Pasadena, 2011b.
- Schiller, C. L., Bozem, H., Gurk, C., Parchatka, U., Konigstedt, R., Harris, G. W., Lelieveld, J., and Fischer, H.: Applications of quantum cascade lasers for sensitive trace gas measurements of CO, CH4, N2O and HCHO, *Appl Phys B-Lasers O*, 92, 419-430, DOI 10.1007/s00340-008-3125-0, 2008.
- Schlosser, E., Brauers, T., Dorn, H. P., Fuchs, H., Haseler, R., Hofzumahaus, A., Holland, F., Wahner, A., Kanaya, Y., Kajii, Y., Miyamoto, K., Nishida, S., Watanabe, K., Yoshino, A., Kubistin, D., Martinez, M., Rudolf, M., Harder, H., Berresheim, H., Elste, T., Plass-Dulmer, C., Stange, G., and Schurath, U.: Technical Note: Formal blind intercomparison of OH measurements: results from the international campaign HOxComp, *Atmos Chem Phys*, 9, 7923-7948, 2009.
- Singh, H. B., Brune, W. H., Crawford, J. H., Jacob, D. J., and Russell, P. B.: Overview of the summer 2004 intercontinental chemical transport experiment - North America (INTEX-A), *J*

Geophys Res-Atmos, 111, Artn D24s01, Doi 10.1029/2006jd007905, 2006.

Snow, J. A., Heikes, B. G., Shen, H. W., O'Sullivan, D. W., Fried, A., and Walega, J.: Hydrogen peroxide, methyl hydroperoxide, and formaldehyde over North America and the North Atlantic, *J Geophys Res-Atmos*, 112, Artn D12s07, Doi 10.1029/2006jd007746, 2007.

Stickler, A., Fischer, H., Williams, J., de Reus, M., Sander, R., Lawrence, M. G., Crowley, J. N., and Lelieveld, J.: Influence of summertime deep convection on formaldehyde in the middle and upper troposphere over Europe, *J Geophys Res-Atmos*, 111, Artn D14308, Doi 10.1029/2005jd007001, 2006.

Tan, D., Faloon, I., Simpas, J. B., Brune, W., Olson, J., Crawford, J., Avery, M., Sachse, G., Vay, S., Sandholm, S., Guan, H. W., Vaughn, T., Mastromarino, J., Heikes, B., Snow, J., Podolske, J., and Singh, H.: OH and HO₂ in the tropical Pacific: Results from PEM-Tropics B, *J Geophys Res-Atmos*, 106, 32667-32681, 2001.

Mastromarino, J., Heikes, B., Snow, J., Podolske, J., and Singh, H.: OH and HO₂ in the tropical Pacific: Results from PEM-Tropics B, *J Geophys Res-Atmos*, 106, 32667-32681, 2001.

Tost, H., Jockel, P. J., Kerkweg, A., Sander, R., and Lelieveld, J.: Technical note: A new comprehensive SCAVenging submodel for global atmospheric chemistry modelling, *Atmos Chem Phys*, 6, 565-574, 2006.

White, J. U.: Long optical paths of large aperture, *J Opt Soc Am*, 32, 285-288, 1942.

Zhang, L., Jacob, D. J., Boersma, K. F., Jaffe, D. A., Olson, J. R., Bowman, K. W., Worden, J. R., Thompson, A. M., Avery, M. A., Cohen, R. C., Dibb, J. E., Flock, F. M., Fuelberg, H. E., Huey, L. G., McMillan, W. W., Singh, H. B., and Weinheimer, A. J.: Transpacific transport of ozone pollution and the effect of recent Asian emission increases on air quality in North America: an integrated analysis using satellite, aircraft, ozonesonde, and surface observations, *Atmos Chem Phys*, 8, 6117-6136, 2008.

Table 1: Atmospheric sources, **sinks** and **cycling** reactions of OH and HO₂ and **calibration sources** of HO_x.

O ₃ + <i>hν</i>	→ O (¹ D) + O ₂ (λ ≤ 340 nm)	R 1
O (¹ D) + H ₂ O	→ 2 OH	R 2
H ₂ O ₂ + <i>hν</i>	→ 2 OH (λ ≤ 400 nm)	R 3
ROOH + <i>hν</i>	→ OH + HO ₂ + HCHO	R 4
HCHO + <i>hν</i>	→ H + CHO (λ ≤ 335 nm)	R 5
H + O ₂ + M	→ HO ₂ + M	R 6
CHO + O ₂	→ HO ₂ + CO	R 7
HCHO + <i>hν</i>	→ H ₂ + CO (λ ≤ 360 nm)	R 8
HO ₂ + HO ₂	→ H ₂ O ₂ + O ₂	R 9
HO ₂ + RO ₂	→ RO ₂ H + O ₂	R 10
OH + NO ₂	→ HNO ₃	R 11
HO ₂ + NO	→ OH + NO ₂	R 12
HO ₂ + O ₃	→ OH + 2 O ₂	R 13
OH + CO + O ₂	→ HO ₂ + CO ₂	R 14
OH + O ₃	→ HO ₂ + O ₂	R 15
OH + CH ₄ + O ₂	→ CH ₃ O ₂ + H ₂ O	R 16
CH ₃ O ₂ + NO	→ CH ₃ O + NO ₂	R 17
CH ₃ O + O ₂	→ HO ₂ + HCHO	R 18
H ₂ O + <i>hν</i>	→ OH + H (λ = 184.9 nm)	R 19
H + O ₂ + M	→ HO ₂ + M	R 6

Table 2: Summarized are mean values of observed and simulated (global model) trace gas mixing ratios and a photolysis frequency. The observations displayed are mean values of the here presented four flights and are separated for convectively (Convective) affected and unaffected (Background) air masses.

	OH [pmol/mol]	HO ₂ [pmol/mol]	NO [pmol/mol]	CO [nmol/mol]	O ₃ [nmol/mol]	H ₂ O ₂ [nmol/mol]	J (O ¹ D) [s ⁻¹]
Background	0.41	15.8	57.5	97.5	81.2	0.69	4.56 10 ⁻⁵
Convective	2.97	14.7	996	107	85.6	1.30	7.57 10 ⁻⁵
Global Model	0.41	8.89	99.3	64.2	102	0.26	3.27 10 ⁻⁵

Table 3: Techniques employed to measure trace species during HOOVER. Abbreviations are explained in the corresponding text.

Species	Technique	Precision	Accuracy	Limit of detection	Time resolution
OH	LIF	0.03 pmol/mol	18 %	0.016 pmol/mol	60 s
HO ₂	LIF	0.42 pmol/mol	18 %	0.33 pmol/mol	60 s
H ₂ O ₂	DEF	8.3 %	14 %	24 pmol/mol	1200 s
ROOH	DEF	6.3 %	21 %	< 24 pmol/mol	1200 s
O ₃	CL	± 1ppt / 4 %	2 %	2000 pmol/mol	30 s
HCHO	QCL	-	8.6 %	300 pmol/mol	120 s
NO	CL	± 8ppt / 7 %	12 %	5 pmol/mol	30 s
CO	QCL	-	1.1 %	200 pmol/mol	2 s
CH ₄	QCL	-	0.57 %	6000 pmol/mol	2 s
J(NO ₂)	FR	1 %	15 %	-	1 s
H ₂ O	Humicap	-	-	100 μmol/mol	30 s

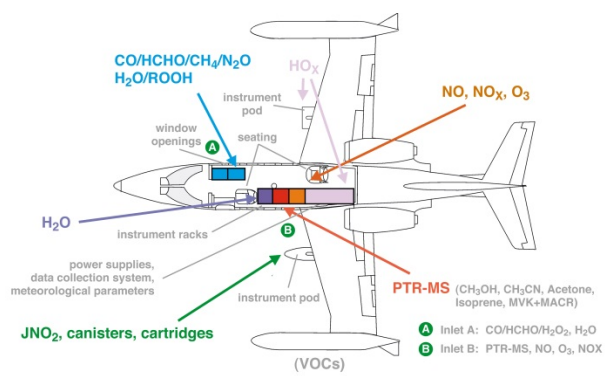


Figure 1: Payload of the Learjet during HOOVER
(© group graphic pool).



Figure 2: HORUS detection axes are mounted in the wing pod below the wing (© group graphic pool).

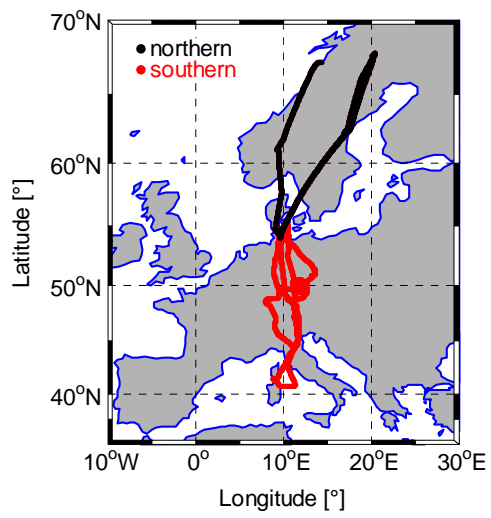


Figure 3: Flight tracks of the HOOVER 2 campaign.

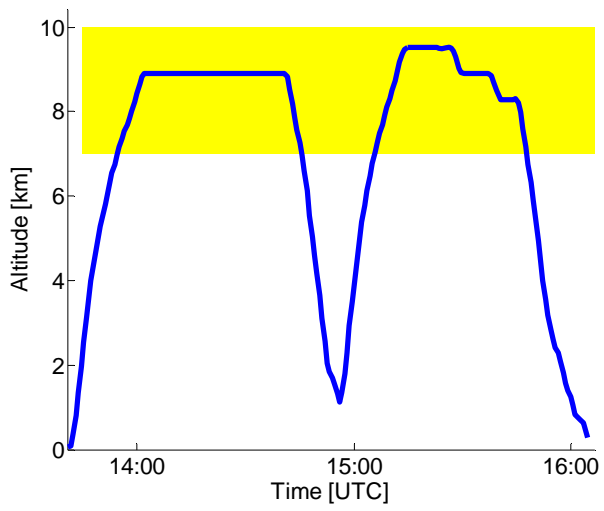


Figure 4: A typical profile of a HOOVER2 flight. Coloured area highlights the upper troposphere.

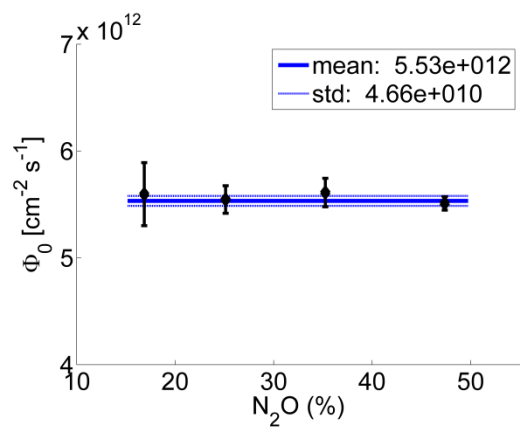


Figure 5: Photon flux Φ_0 calculated from NO measurement for different N_2O mixing ratios.

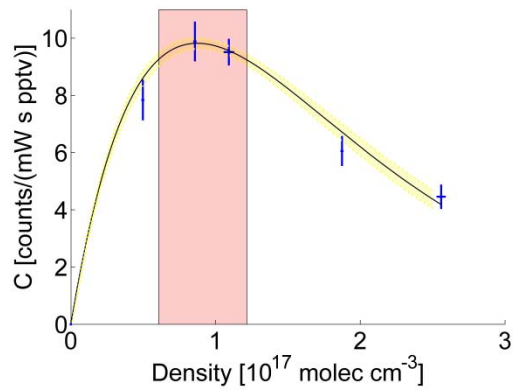


Figure 6: Pressure dependency of the instrument sensitivity. Highest sensitivity is found between 2.5 and 5 mbar in the highlighted red area. Points shown are mean values of individual calibrations; the error bars indicate the variability between the individual calibrations. The black line represents a chi-square fit and the yellow area indicates the uncertainty

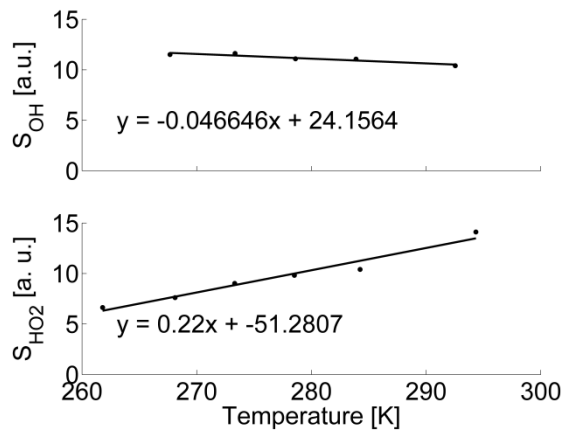


Figure 7: A calibration at different temperatures was conducted to study the effect of temperature dependent surface losses of HO₂ within the inlet and detection system of HORUS under upper tropospheric conditions. Here the signal S which is normalized to laser power and time is shown as a function of temperature.

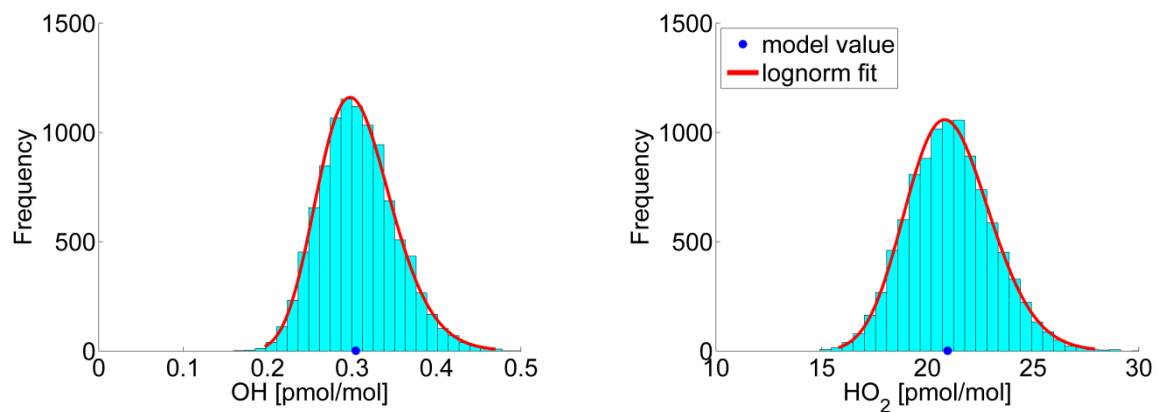


Figure 8: Distribution of the OH- and HO₂-mixing ratio derived from Monte-Carlo-simulation of the data set observed in the upper troposphere over Europe, see section 4b for details. The model value indicates the simulated mixing ratio resulting from the model run, when no Monte-Carlo-variation was applied.

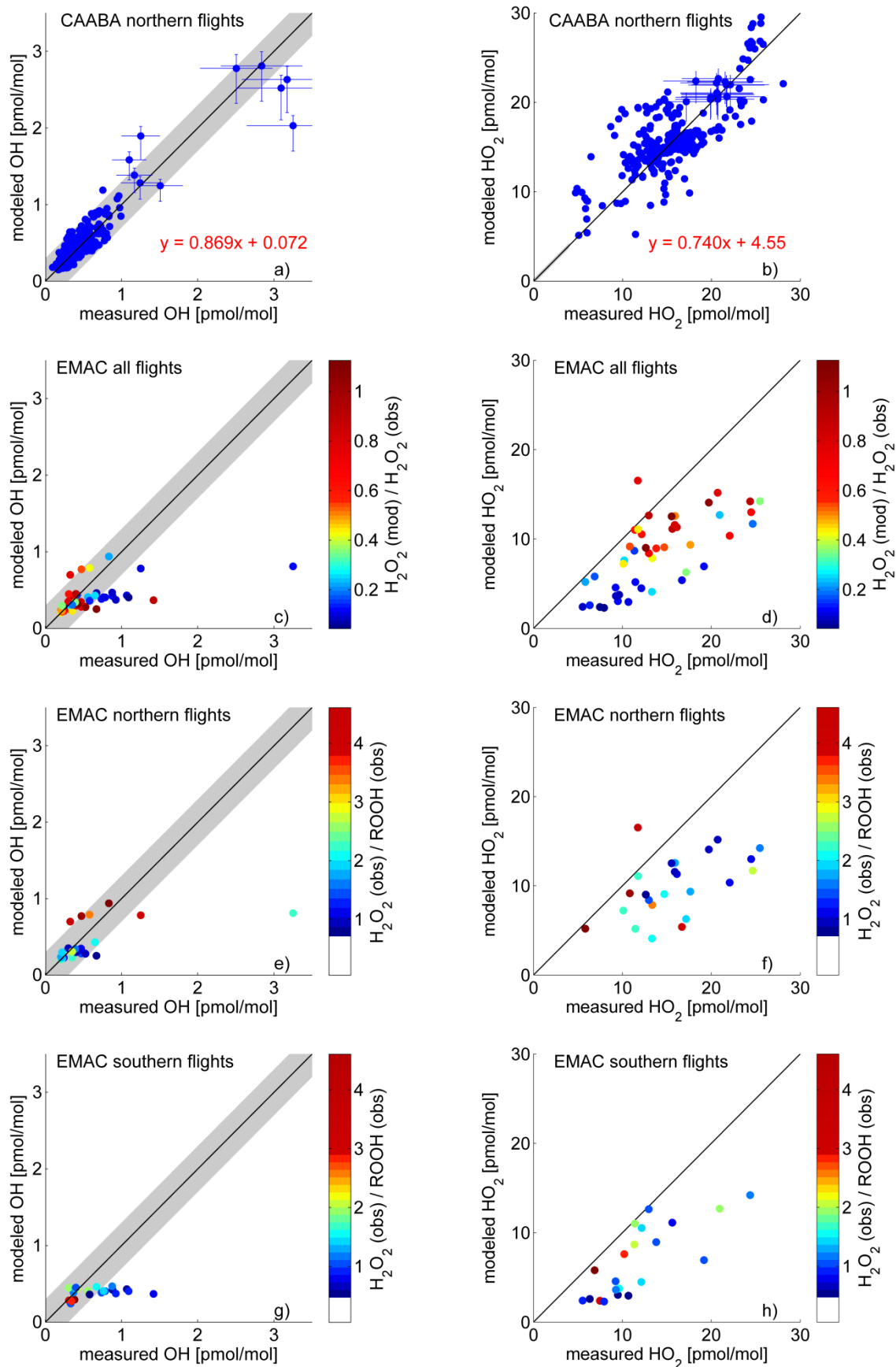


Figure 9: Comparison of model calculations to observed OH and HO₂. CAABA reproduces the observed OH mixing ratios within ± 0.3 pmol/mol (shaded area) in the upper troposphere. The 1:1 line is given in black, the equation given in red indicates the result of a linear fit. In subplots a) and b) a limited number of errorbars is shown to improve readability.

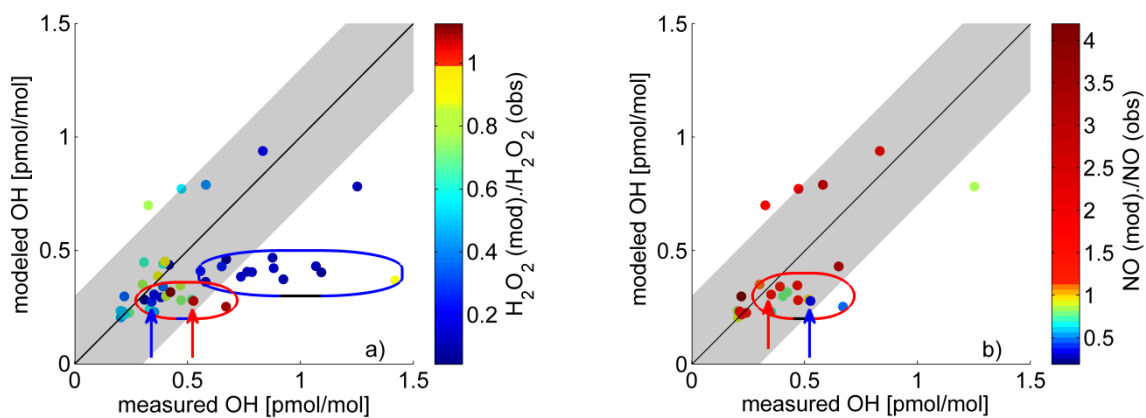


Figure 10: Highlighted are underestimated OH mixing ratios at underestimated H_2O_2 mixing ratios (blue ellipse). Within the red ellipse some data points show slightly underestimated OH at relatively well reproduced H_2O_2 but severely underestimated NO, while at other times OH was reasonable reproduced even though H_2O_2 mixing ratios in the model were much too low and NO was overestimated. Figure 10a is a cut-out of Figure 9c. To highlight the statement the colour coding was adapted.

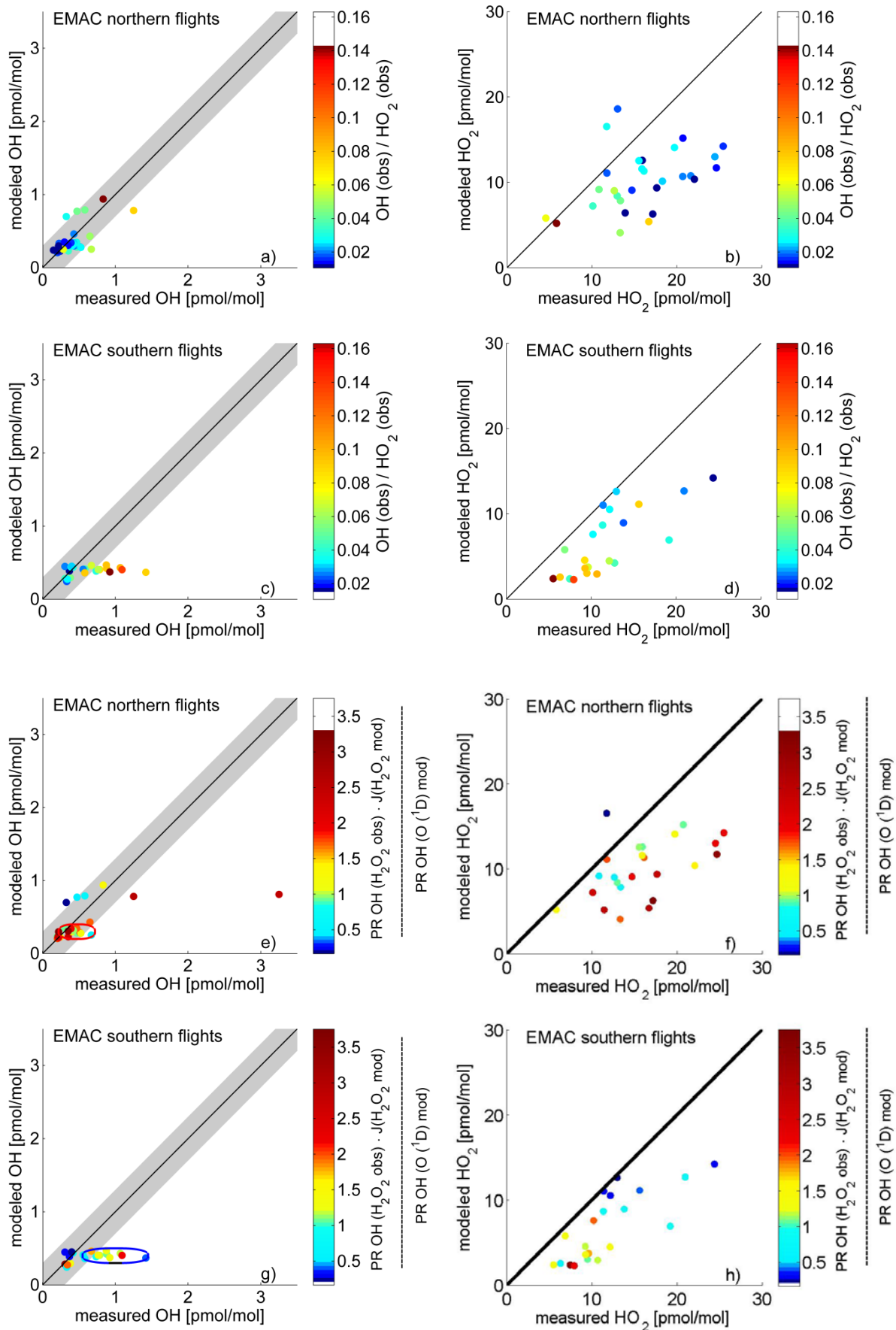


Figure 11: Comparison of model simulation to observed OH and HO₂ mixing ratios. Colour coding highlights the conversion ratio and the ratio of primary production rates. The 1:1 lines are given in black.